Influence of the plasma environment on atomic structure using an ion-sphere model

Madeny Belkhiri, Christopher J. Fontes, and Michel Poirier

Influence of the plasma environment on atomic structure using an ion-sphere model

Madeny Belkhiri* and Christopher J. Fontes

Computational Physics Division, Los Alamos National Laboratory,

Los Alamos, New Mexico 87545, USA

Michel Poirier

CEA, IRAMIS, Laboratoire Interactions,

Dynamique et Lasers, Centre d'Études de Saclay,

F91191 Gif-sur-Yvette Cedex, France.

1

Abstract

Plasma environment effects on atomic structure are analyzed using various atomic structure codes. To monitor the effect of high free-electron density or low temperatures, Fermi-Dirac and Maxwell-Boltzmann statistics are compared. After a discussion of the implementation of the Fermi-Dirac approach within the ion-sphere model, several applications are considered. In order to check the consistency of the modifications brought here to extant codes, calculations have been performed using the CATS code in its Hartree-Fock or Hartree-Fock-Slater form and the parametric potential code FAC. The ground-state energy shifts due to the plasma effects for the six most ionized aluminum ions have been calculated using the FAC and CATS codes and fairly agree. For the intercombination resonance line in Fe^{22+}, the plasma effect within the Uniform Electron Gas Model results in a positive shift that agrees with the MCDF value of Saha *et al*. Last, the present model is compared to experimental data in titanium measured on the terawatt ASTRA facility and provides values for electron temperature and density in agreement with the MARIA code.

* madeny.belkhiri@lanl.gov; Corresponding author

I. INTRODUCTION

Many atomic structure codes are available to obtain an accurate description of energy levels and transitions, employing such methods as Hartree-Fock, Dirac-Fock, or parametric potentials. However, these codes typically do not include plasma-environment effects. These are often taken into account after the fact, within a kinetics (or collisional-radiatve) code by way of energy shifts computed from various semi-classical formulas, the most popular being that of Stewart and Pyatt [1]. To circumvent this limitation, we have in earlier works [2–4] shown that plasma effects may be included in the Flexible Atomic Code (FAC) [5] within the ion-sphere formalism (ISF). However, our previous work relied only either on this code and on a direct integration of the Schrödinger radial equation in the H-like case, and the comparison with the existing literature using ISF was limited to ions with a single bound electron.

The goal of the present work is to generalize this approach in three directions. First, our earlier work relied on a Maxwell-Boltzmann statistics to describe the free electrons, which is not correct when their density is high or when their temperature is low. Therefore we provide an analysis of the improvement brought by the use of Fermi-Dirac statistics. Second, we have now included the plasma environment effect within the ISF in the Los Alamos CATS (Cowan ATomic Structure) code [6, 7] based on Cowan's work [8]. It is instructive to compare results from FAC and CATS since they rely on somewhat different hypotheses. FAC is a fully relativistic code based on the fit of free parameters in the potential and on a local approximation of the exchange interaction based on standard Dirac-Fock-Slater method. CATS relies on a semi-relativistic self-consistent potential using a non-local Hartree-Fock (HF) or local Hartree-Fock-Slater (HFS) description for exchange. Since we are using the semi-relativistic option in this work, we will use the HFR acronym to denote the HF calculations. The last new aspect of this paper is the presentation of comparisons of results obtained with FAC, CATS, and other codes from the literature (MCDF, SOBOLEV/MARIA) for complex ions, while in our previous work comparisons mostly dealt with the hydrogen-like case.

The Debye-Hückel model [9, 10] is one of the most commonly used formalisms to take into account the plasma effects in atomic structure calculations. However, the validity of this approach is questionable, as mentioned, for example, by Nguyen et al. [11] and Iglesias and Lee [12]. Indeed, the Debye-Hückel model is valid when the correlation time of the ion is much longer than the lifetime of excited atomic states. So this perturbative approach is, at best, limited to weakly coupled plasmas and is not relevant for the modeling of high density plasmas considered in this work. If we set aside the Debye-Hückel model, the first significant effort to account for the plasma environment effect was made through Thomas-Fermi approach [13]. The next important step is due to Rozsnyai [14], who computed energy levels and analyzed the equation of state in a dense plasma using a relativistic Thomas-Fermi approach. Since then, several approaches have been developed, which are mostly related to the Kohn-Sham density functional theory.

In the ion-sphere model, the ion is enclosed in a spherically symmetric cell that contains the exact number of electrons to ensure neutrality. Such models define an electron-density distribution that obeys self-consistency equations or a simpler hypothesis such as uniform density. In its simplest form, assuming exact cancellation of the free-electron and other-ion densities beyond the Wigner-Seitz sphere, the ion-sphere model has been extensively used (see Refs. [14–20], to quote just a few) to obtain energy levels and transition rates of ions in plasmas. In other variants, the ion is immersed in an infinite polarizable medium, also called jellium. Asymptotically, the positive and negative charges cancel out each other to form a neutral background. The high-temperature limit of such models is the popular Debye-Hückel theory [9, 21, 22]. A recent approach of this type is the Variational Average Atom in Quantum Plasma by Blenski and Piron [23, 24].

This manuscript is organized as follows: In section II we briefly recall the basic equations of the ion-sphere model with an emphasis on the Fermi-Dirac approach. In section III we present the numerical implementation of the TF approach in the HFS

4

and HFR paths of the CATS code. In section IV we compare energies obtained with a Thomas-Fermi approach using the Maxwell-Boltzmann and Fermi-Dirac distributions. In the same part we present three comparisons on several ions. Firstly, we compare FAC and CATS results for aluminum-ion ground state. Then we compare our results with an independent calculation using the uniform electron gas model (UEGM) with a MCDF code [18]. The last ion studied is He-like titanium, for which a published experiment [25] exhibits a plasma density effect on the He-α line. We end this manuscript with concluding remarks.

Atomic units are used throughout.

II. ION-SPHERE MODEL

The general category of ion-sphere models includes models that assume a neutral cell containing a central ion surrounded by its environment. Moreover, one assumes that the free-electron density exactly cancels the ion density beyond the ion-sphere radius. In this approach the plasma potential is calculated using the Poisson equation. The difference between the various ion-sphere models lies in the way the density of free electrons is determined. We present here the Thomas-Fermi (TF) approach using a Fermi-Dirac distribution.

A. Thomas-Fermi approaches

The Thomas-Fermi model has been discussed in a series of papers [3, 11, 13, 17, 26, 27]. We briefly recall the main equations of the ion-sphere model. The neutrality assumed inside the ion-sphere sphere with radius R_0 is defined by

$$4\pi R_0^3 N_e / 3 = Z_f, \tag{1}$$

5

where N_e is the average free-electron density and Z_f the number of free electrons. The free-electron density outside of the sphere is

$$n_e(r) = 0 \text{ for } r \geq R_0. \tag{2}$$

In order to comply with the definition of the average electron density N_e, one imposes the condition

$$4\pi \int_0^{R_0} dr\, r^2 n_e(r) = Z_f. \tag{3}$$

In the CATS and FAC codes, the free-electron density $n_e(r)$ can follow three distributions: a uniform density, the Maxwell-Boltzmann or the Fermi-Dirac distribution. The case of a uniform density and Maxwell-Boltzmann distribution have been discussed in [2, 3] only for FAC. In the following subsection we present the implementation of the Fermi-Dirac distribution in CATS and FAC.

B. Fermi-Dirac distribution

If the free electrons are degenerate, the use of the Fermi-Dirac distribution is preferable. In that case the free-electron density is

$$n_e(r) = \frac{1}{\pi^2} \int_{p_0(r)}^{\infty} dp \, \frac{p^2}{e^{\left(\frac{p^2}{2} + V(r) - \mu\right)/kT_e} + 1}, \tag{4}$$

where μ is the chemical potential, $p_0(r) = (-2V(r))^{1/2}$ in the case of an attractive potential, and $V(r)$ is

$$V(r) = \begin{cases} -\frac{Z}{r} + V_{ee}(r) + V_{\text{pl}}(r) + V_{\text{relat}}(r) & r \leq R_0 \\ 0 & r > R_0, \end{cases} \tag{5}$$

where V_{ee} accounts for all interactions between bound electrons, including nucleus screening by bound electrons and the exchange interaction. The term V_{relat} represents the relativistic corrections, we note that this term is absent from the FAC code since it is a fully relativistic code. The difference between the Maxwell-Boltzmann approach and

6

Fermi-Dirac distribution lies in the presence of the chemical potential μ. This parameter is determined by the neutrality condition.

Assuming a change of variable $p \equiv (2kT_e x)^{1/2}$, the density becomes

$$n_e(r) = \frac{4}{\sqrt{\pi}} \left(\frac{kT_e}{2\pi} \right)^{3/2} \int_{x_0}^{\infty} dx \, \frac{x^{1/2}}{e^{x-x_0-\mu/kT_e}+1}, \tag{6}$$

where $x_0 = -V(r)/kT_e$. Finally, we can write equation (6) as

$$n_e(r) = 2\lambda_{th}^{-3} \mathscr{F}_{1/2} \left(-\frac{V(r)}{kT_e} + \frac{\mu}{kT_e}, -\frac{V(r)}{kT_e} \right). \tag{7}$$

The function $\mathscr{F}_{1/2}(x,y)$ is called the incomplete Fermi-Dirac integral and λ_{th} is the De Broglie thermal wavelength defined by

$$\lambda_{th} = \left(\frac{2\pi}{kT_e} \right)^{1/2}. \tag{8}$$

The last equation required to obtain the plasma potential and the electron density is the Poisson equation, which can be written in integral form as

$$V_{\text{pl}}(r) = 4\pi \left(\frac{1}{r} \int_0^r ds \, s^2 n_e(s) + \int_r^{R_0} ds \, s \, n_e(s) \right). \tag{9}$$

Two iterative loops have to be done in this case: one to obtain the chemical potential μ, which is an internal loop, and the other one (external loop) to obtain the correct density due to the sphere neutrality. The numerical procedure is detailed in subsection III B.

III. ATOMIC STRUCTURE CALCULATIONS INCLUDING THE PLASMA POTENTIAL

We present in this section the modifications that were made in the CATS and FAC codes, which in their standard versions do not take into account the plasma environment. Using the modified form of these codes, we obtain energy levels, wave-functions and radiative rates that take into account the plasma environment within the ion-sphere model.

A. Implementation of plasma density effects in CATS and FAC

The CATS code is used to generate solutions of the Schrödinger equation with relativistic corrections. Since the plasma potential is spherically symmetric, it is only necessary to modify the radial equation:

$$\frac{d^2 R_{n,l}}{d^2 r} + 2 \left(E_{n,l} - V(r) - \frac{l\,(l+1)}{2r^2} \right) R_{n,l} = 0, \tag{10}$$

where n is the principal quantum number, l the orbital quantum number, $E_{n,l}$ is the energy eigenvalue and $R_{n,l}$ the radial wave-function. The total potential acting on the electron is

$$V(r) = -\frac{Z}{r} + V_{\text{pl}} + V_{ee} + V_{\text{relat}}. \tag{11}$$

We note that the CATS code does not report the orbital binding energy as the actual eigenvalue of equation (10). Instead, the binding energies are calculated by constructing the appropriately averaged value of the kinetic, nuclear and electron-electron terms (see for example, equation (6.13) of Cowan [8]). The goal of this procedure is to obtain more accurate energies when the local-exchange (HFS) approximation is used. When the non-local (HFR) approach is used, this procedure reproduces the eigenvalues from equation (10).

We have to mention an important point concerning the asymptotic behavior for the active electron. The expected asymptotic charge experienced by an active electron should be $(Z-N_b+1)$ when the plasma effects are not considered. However, when dealing with the local-exchange approximation employed in the HFS method, the asymptotic behavior is $(Z-N_b)$. In the ion-sphere approach the active electron experiences a $(Z - N_b + 1 + Z_f) = 1$ charge outside the ion sphere, which is not consistent with the HFS method. To solve this problem, the Latter tail cut off [8, 28] is applied only to the HFS potential, rather than to the sum of the HFS and the plasma potentials.

Concerning FAC, the implementation of the Fermi-Dirac approach is similar to that described above for the HFS method.

8

B. Plasma potential with a Fermi-Dirac distribution of free electrons

To start the first iteration, we use a uniform density distribution of free electrons and deduce the plasma potential; this iteration produces the UEGM potential denoted by $V^{(0)}$. For the first guess of the chemical potential, labeled $\mu(0)$, we use the value of an ideal gas at high temperature, i.e.

$$\mu(0) = kT_e \log \left(\frac{3 Z_f \lambda_{th}^3}{8 \pi R_0^3} \right). \tag{12}$$

We recall that an internal and external loop are necessary. We denote the external loop with the index i and the internal loop with the index k. The internal loop is used to calculate the chemical potential $\mu(i, k)$ and the external loop for the density $n_e^{(i)}(r)$.

To determine the next i^{th} value of μ, we use a Newton iterative method. We calculate the free charge $Z_f^{i,k}$ for iteration (i, k) according to

$$8 \pi \lambda_{th}^{-3} \int_0^{R_0} dr \, r^2 \mathscr{F}_{1/2} \left(-\frac{V^{(i)}(r)}{kT_e} + \frac{\mu(i, k)}{kT_e}, -\frac{V^{(i)}(r)}{kT_e} \right) = Z_f^{i,k}. \tag{13}$$

We suppose at the next iteration on k, the value $Z_f^{i,k+1}$ that we obtain is the exact free charge Z_f, i.e.

$$8 \pi \lambda_{th}^{-3} \int_0^{R_0} dr \, r^2 \mathscr{F}_{1/2} \left(-\frac{V^{(i)}(r)}{kT_e} + \frac{\mu(i, k+1)}{kT_e}, -\frac{V^{(i)}(r)}{kT_e} \right) = Z_f. \tag{14}$$

To obtain the expression for $\mu(i, k+1)$, we assume that the variation of $\mathscr{F}_{1/2}(x, y)$ can be approximated by the first-order discretization

$$\mathscr{F}_{1/2}(x_{k+1}, y) - \mathscr{F}_{1/2}(x_k, y) = (x_{k+1} - x_k) \frac{\partial}{\partial x} \mathscr{F}_{1/2}(x, y) \Big|_{x=x_k}. \tag{15}$$

Therefore, we obtain the new chemical potential $\mu(i, k+1)$ via the following expression:

$$\begin{aligned} (\mu(i, k+1) - \mu(i, k)) \int_0^{R_0} dr \, r^2 \frac{\partial}{\partial x} \mathscr{F}_{1/2} \left(-\frac{V^{(i)}(r)}{kT_e} + \frac{\mu(i, k)}{kT_e}, -\frac{V^{(i)}(r)}{kT_e} \right) \\ = \frac{kT_e \lambda_{th}^3}{8\pi} \left(Z_f - Z_f^{i,k} \right). \end{aligned} \tag{16}$$

9

The partial derivative of the Fermi-Dirac integral can be calculated by

$$\frac{\partial}{\partial x}\mathscr{F}_j\left(x,y\right) = \frac{1}{\Gamma\left(j+1\right)}\frac{y^j}{e^{y-x}+1} + \mathscr{F}_{j-1}\left(x,y\right).$$ (17)

For the computation of the Fermi-Dirac integral, we use the algorithm developed by Goano [29]. The internal loop has converged when the required accuracy $|\mu(i, k+1) - \mu(i,k)| < \epsilon$ is reached. The default value of ϵ is 10^{-12}. Once the chemical potential is obtained, the process to obtain the density $n_e(r)$ and the potential $V_{\text{pl}}^{(i)}(r)$ is

$$V^{(i)}(r) = -\frac{Z}{r} + V_{ee}(r) + V_{\text{relat}}(r) + V_{\text{pl}}^{(i)}(r),$$ (18)

$$n_e^{(i)}(r) = 2\lambda_{th}^{-3}\mathscr{F}_{1/2}\left(-\frac{V^{(i)}(r)}{kT_e} + \frac{\mu(i,k+1)}{kT_e}, -\frac{V^{(i)}(r)}{kT_e}\right).$$ (19)

$$Z_f = 4\pi\int_0^{R_0} dr\, r^2 n_e^{(i)}(r),$$ (20)

$$V_{\text{pl}}^{(i+1)}(r) = 4\pi\left(\frac{1}{r}\int_0^r ds\, s^2 n_e^{(i)}(s) + \int_r^{R_0} ds\, s\, n_e^{(i)}(s)\right),$$ (21)

where $\mu(i, k+1)$ is the converged value of the chemical potential at the i-th step of the outer iteration. The convergence is controlled by monitoring the variation of the density on the ion-sphere sphere $|n_e^{(i)}(R_0) - n_e^{(i-1)}(R_0)|$, ending the iterations when this difference falls below a given tolerance ε. We found that $\varepsilon = 10^{-8}$ in atomic units produced the self-consistent potential with a fair accuracy, and that the procedure converged in most cases in less than 12 iterations. This part of the procedure is identical to the one presented previously for the case of a Maxwell-Boltzmann distribution [3].

We point out that in the CATS and FAC codes the ion-sphere radius R_0 does not typically correspond to a specific point on the integration mesh. In the appendix A we show that a linear interpolation is sufficient to adress this issue.

IV. RESULTS

A. Maxwell-Boltzmann vs Fermi-Dirac

The difference between Maxwell-Boltzmann and Fermi-Dirac statistics is illustrated in Figure 1, where we have plotted the numerical results for the plasma potential for the case of H-like neon at 1 eV and $N_e = 10^{24}$ cm^{-3}. In this case, the degeneracy factor $\gamma = N_e \lambda_{th}^3$ is 331 and the plasma coupling parameter [30] is $\Gamma = 1115.9$, making the free electrons degenerate and resulting in curves that do not overlap.
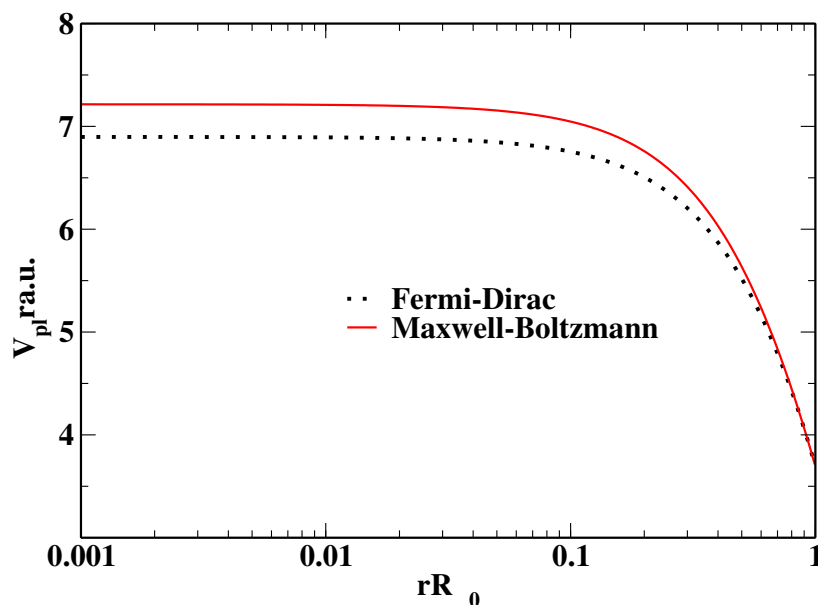

FIG. 1. Influence of different free-electron distributions on the self-consistent plasma potential for H-like neon at $T_e = 1$ eV and $N_e = 10^{24}$ cm^{-3}. The electron distance to the nucleus, r, is expressed in units of the ion-sphere radius $R_0 = 2.438\, a_0$. The potential is obtained from CATS using the HFS path.

The plasma potential with the Fermi-Dirac distribution is weaker than the Maxwell-Boltzmann one. Taking into account the Pauli principle reduces the free-electron concentration for $r \simeq 0$ and therefore the screening of the nuclear potential. Accordingly

11

Temperature	Maxwell-Boltzmann	Fermi-Dirac
1 eV	193.85	185.58
100 eV	167.72	167.39
1000 eV	154.31	154.31

TABLE I. Energy shift in eV for the 1s level of H-like neon at an average electron density of $N_e = 10^{24}$ cm^{-3} from CATS (HFS).

one must recall that the TF model, which accounts for such polarization of the free electrons, leads to a stronger plasma effect than the UEGM. We can draw an analogy with the theory of atomic structure, which deals only with bound electrons. In this latter case, the Pauli principle is taken into account through the exchange interaction, for which the contribution to the average energy of a configuration is negative. Therefore, it seems reasonable to expect the same influence when Fermi-Dirac statistics is used.

We provide a comparison of shifted energies for H-like aluminium calculated with the CATS HFS option in Table I; the HFR results are identical (not shown). We clearly see in this table that the binding energies decrease less with temperature when the Fermi-Dirac distribution is used, compared to the Maxwell-Boltzmann distribution. As explained above, this behavior is a consequence of the free-electron degeneracy.

B. Results on energies

In a previous article [2], the energy shift due to the plasma effect given by FAC has been verified for H-like ions using an analytical formula. When dealing with more than one bound electron, further numerical comparison is desirable. Therefore, to check the results of our calculations we offer a comparison between FAC and CATS (both HFS and HFR results).

Ground states	Binding energy shift in eV			Relative difference in %	
	FAC	CATS(HFS)	CATS(HFR)	FAC vs HFS	FAC vs HFR
$1s^2$	193.330	193.286	193.299	0.025	0.016
$1s^2 2s^1$	173.975	173.895	173.885	0.046	0.052
$1s^2 2s^2$	160.869	160.727	160.744	0.088	0.077
$1s^2 2s^2 2p^1$	148.427	148.460	148.661	0.022	0.158
$1s^2 2s^2 2p^2$	134.120	134.193	134.338	0.055	0.16

TABLE II. Shift of the binding energies due to the plasma potential of Al ground state ions at an average electron density of $N_e = 10^{24}$ cm^{-3} and a temperature $kT_e = 100$ eV with a Fermi-Dirac distribution. The plasma potential shifts the energies upward. Therefore the binding energies are reduced by the plasma effect.

1. Aluminum ions

The most relevant comparison is between FAC and CATS using the HFS approximation because both rely on a local potential for the exchange interaction. In Table II, we provide the energy shift of the binding energies for different ground states of the aluminum ions. As we can observe, the results between all the codes are satisfying, especially between FAC and CATS (HFS). The relative error is very small and reaches the numerical precision of the codes (a maximum of 5 digits for energies). As expected, the agreement between FAC and CATS (HFR) is not as good as the CATS (HFS) when increasing the number of bound electrons. This is because the local-exchange approximation is becoming less valid with an increase in the number of bound electrons. However, the agreement is still very good.

As a completely independent check, we also compare our calculations of He-like aluminium with the work of Sil et al. [20]. In their paper, they present configuration-average energies for transitions of the type $1s^2 - 1snp$ using the UEGM. The main difference with the present work is that they require the wave-function to be zero at

the ion-sphere radius. In Table III, we compare the shift of those transition energies obtained from FAC and CATS (HFR), using the UEGM, with their relativistic results. We note that CATS is not a fully relativistic code, but the HFR option includes the lowest-order relativistic corrections [8]. Futhermore, for aluminum we do not expect a strong relativistic effect. We can estimate that the relativistic corrections are of the order of $Z^2\alpha^2$ ($\sim 1/100$ for Al ions). The agreement of the plasma shift is good at a density of $N_e = 10^{23}$ cm^{-3} between FAC and CATS. However, the agreement between our codes (FAC and CATS) and Sil et al. is not as good, especially for the $1s^2 - 1s2p$ transition. It is difficult to find an explanation for this behavior. We do not believe that the difference in the choice of boundary condition has any influence on this specific transition. Indeed, at a given density, the higher values of n are more sensitive to the plasma effect, which leads to a stronger effect on the wave-function. Thus, the choice of boundary condition for the wave-function is expected to have the strongest effect for higher values of n. We develop this point in the next subsection IV B 2. Therefore, we expected that the disagreement in the shift should have increased with an increase in the principal quantum number n, contrary to the observed trend in Table III. We note that at higher free-electron densities, i.e. $N_e = 10^{24}$ cm^{-3}, the relative difference in the energy shift for the $1s^2 - 1s2p$ transition between FAC and the work of Sil et al. is about 4.68%, while the relative difference between FAC and CATS is only about 0.11%. So the discrepancy between our shifts and those of Sil et al. increases with density. Overall, the same quantitative agreement described for aluminum is found for the other elements (carbon and argon) that are present in the reference [20]. Similar trends are also observed for the transitions in H-like ions reported by Battacharyya et al. [19].

Transitions	Energy shift in eV			Relative difference in %	
	FAC	CATS(HFR)	Sil et al. [20]	FAC vs CATS(HFR)	FAC vs [20]
$1s^2 - 1s2p$	0.1547	0.1544	0.1605	0.19	3.75
$1s^2 - 1s3p$	1.0268	1.0262	1.0476	0.06	2.03
$1s^2 - 1s4p$	3.5485	3.5520	3.6055	0.10	1.61
$1s^2 - 1s5p$	9.8662	9.8966	9.7058	0.31	1.63

TABLE III. Shift of energies for the $1s^2 - 1snp$ transitions in Al^{11+} due to the plasma potential at an average electron density of $N_e = 10^{23}$ cm^{-3} using the UEGM. The results from the work of Sil et al. [20] are taken from their relativistic calculations.

2. Beryllium-like ions

We may also perform another comparison with the work of Saha et al. [18] which uses a multiconfiguration Dirac-Fock (MCDF) calculation within the ion-sphere model. In their paper, the chosen ion-sphere model is the UEGM. This model is suitable when the temperature is high enough to assume a uniform density of free electron. In their ion-sphere model an additional assumption is made on the wave-functions. They impose the wave-function to be zero on the ion-sphere. We believe that this assumption — though of little consequence here as will be discussed later — is not suitable because it leads to unphysical behavior. Indeed, the cancellation of the wave-function on R_0 is equivalent to an infinite potential at the ion-sphere radius.

In the work of Saha et al. [18], the energy shift caused by the plasma is given for the $2s^2 - 2s2p\,^3P_1$ intercombination line and the $2s^2 - 2s2p\,^1P_1$ resonance line of beryllium-like ions for different elements (O, Ne, Si, Ar, Fe, Mo). To lead the comparison with their work, we have chosen the ion Fe^{22+}.

We firstly focus our attention on the intercombination line. As we observe in Table IV the agreement between the three codes is satisfactory (less than a $1\,\%$ difference).The agreement between the codes and the NIST value [31] is of similar quality. Usually the

	FAC	CATS (HFS)	CATS (HFR)	MCDF	NIST
Unperturbed energy in units of eV	47.1104	46.8781	47.1323	47.1181	47.0055
Plasma shift in units of eV $\quad N_e = 10^{23}$	0.01331	0.01383	0.01381	0.01327	
$N_e = 10^{24}$	0.1327	0.1347	0.1344	0.1327	
$N_e = 5 \times 10^{24}$	0.6647	0.6712	0.6698	0.6647	

TABLE IV. Unperturbed energy (i.e., for $N_e = 0$) and plasma energy shift at various electron densities for the $2s^2 - 2s2p\,^3P_1$ intercombination line of Fe^{22+}. Electron densities N_e are in cm^{-3}. The plasma shift is computed using the UEGM. The MCDF calculations are from Saha et al [18], the NIST data from Kramida et al [31].

plasma effect shifts the transition energies downward for ions with few electrons, so it is noteworthy to mention that this case behaves differently. This issue was previously discussed in [32], in which the terminology blue and red shift was applied to upward and downward shifted energies, respectively. The results from CATS are slightly different from FAC and MCDF because it is a semi-relativistic code, while the results of FAC and the MCDF code of Saha et al. [18] are very similar, despite the assumption of cancellation of the wave-function on the ion-sphere in the latter calculations. This agreement is good because, at the density presented in Table IV, the wave-functions have converged to zero at a distance much less than the ion-sphere radius ($R_0 = 1.921\ a_0$). Therefore, in this case, no difference should be expected between the two models. In Figure 2 we have plotted the set of wave-functions generated with CATS (HFR) that were used to represent the $1s^2 2s^2$ and $1s^2 2s2p\,^3P_1$ levels, which supports our argument.

Concerning the resonance line, the results shown in Table V are not as good as those of the intercombination line. The biggest disagreement is $\sim 3.7\%$ between FAC and MCDF in most of the cases.

For completeness, when studying elements with lower values of Z, we note that the discrepancy between FAC and MCDF increases. We find a $6.7\ \%$ difference on the plasma shift for O^{4+} ions between FAC and MCDF, and $0.46\ \%$ for Mo^{38+}. We
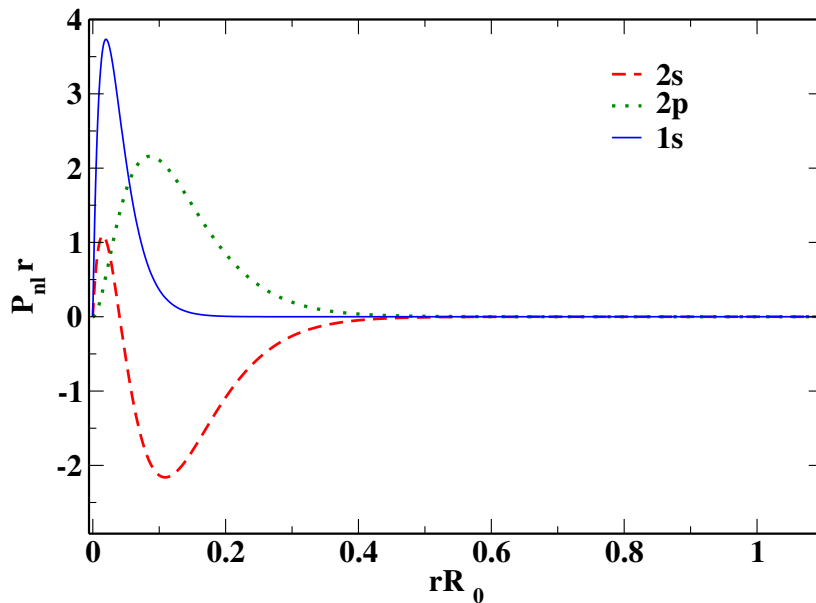
FIG. 2. Radial wavefunctions for the $1s^2 2s^2$ and $1s^2 2s2p\ {}^3P_1$ levels of Fe^{22+}, at a density of $N_e = 5 \times 10^{24}$ cm^{-3} calculated with the UEGM. The electron distance to the nucleus, r, is expressed in units of the ion-sphere sphere radius $R_0 = 1.921\ a_0$. The wave-functions have been computed from CATS (HFR).

emphasize that this behavior is only observed for the resonance line. This discrepancy might be explained by the fact that the wave-functions of FAC may not converge to the non-relativistic wave-functions. This type of non-convergence has been observed and discussed by Kim et al. [33] for MCDF codes. However we point out that in the latter paper the discrepancy is observed for the intercombination line, while in our case it concerns the resonance line. We do not discuss this possibility in more detail here, since it is beyond the scope of this article.

3. He-α line for Titanium

In the last case, we compare our work with an experiment published by Khattak et al. [25] on titanium. This experiment was performed at the Rutherford Appleton

	FAC	CATS (HFS)	CATS (HFR)	MCDF	NIST
Unperturbed energy in units of eV	94.8552	92.4145	92.5428	93.848	93.2869
Plasma shift in units of eV $N_e = 10^{23}$	0.01193	0.01256	0.01254	0.01239	
$N_e = 10^{24}$	0.11941	0.12185	0.12161	0.12386	
$N_e = 5 \times 10^{24}$	0.59770	0.60656	0.60543	0.62077	

TABLE V. Unperturbed energy (i.e., for $N_e = 0$) and plasma energy shift at various electron densities for the $2s^2 - 2s2p\,{}^1P_1$ resonance line of Fe^{22+}. See Table IV for details.

Laboratory using the terawatt short pulse laser facility ASTRA. This work reported a red shift of the Ti He-α line which is the highest charge state measured (the average charge of the plasma being $Z^* \simeq 20$). In that paper the titanium foil was irradiated at on optimum focus and at an offset of 100 μm from the best focus. Therefore two He-α line shifts were reported. In the case of the optimum focus, the reported line shift was 3.4 eV, while in the second focus the measured line shift was 1.8 eV. The unshifted He-α line was taken to be at 4749.73 eV in [25], as provided by Beiersdorfer et al [34]. A similar value of 4749.85 eV was given by Chantler et al [35]. We point out that the FAC code provides an unshifted value of 4749.34 eV. The unshifted value of CATS (HFR and HFS) is 4753.48 eV.

In order to evaluate the density and the temperature, two simulations were carried out in the article. The first simulation was realized by the hydrodynamic code HYADES [36] and post-processed with the collisional-radiative code SOBOLEV [37]. This simulation concluded that the plasma density exceeded $N_e = 10^{24}$ cm^{-3} with a temperature above 3000 eV in the case of the optimum focus. In the second focus a temperature of well below 1000 eV and density lower than $N_e = 10^{24}$ cm^{-3} was suggested. The second simulation was performed with the spectral simulation code MARIA [38]. For the optimum focus, the prediction of MARIA is close to the first simulation. For the second focus, the estimate range of temperature is $500 - 1000$ eV and an electron density closer

18

to 10^{23} cm^{-3} than 10^{24} cm^{-3}.

From our numerical simulation with FAC using the ion-sphere model (Fermi-Dirac distribution), a line shift of 3.4 eV for the He-α is obtained for an electron density of 4.2×10^{24} cm^{-3} with an electron temperature of 3000 eV. The density and temperature used in our model are in good agreement with those mentioned in the paper of Khattak et al. [25]. For the second focus, a line shift of 1.8 eV is found at an electron density of $N_e = 10^{24}$ cm^{-3} with an electron temperature of 587 eV. The temperature falls within the range predicted by the code MARIA. However our density is higher than the one obtained with the code MARIA [38].

Concerning CATS (both HFR and HFS), we obtain very similar results compared to FAC. A shift of 3.4 eV for the He-α line is obtained for an electron density of $N_e = 4.1 \times 10^{24}$ cm^{-3} with an electron temperature of 3000 eV. For the second focus the density and temperature used with CATS are exactly the same as the ones obtained with FAC.

V. SUMMARY

Using a Thomas-Fermi description of the free-electron density, we have been able to describe plasma environment effects within the Hartree-Fock or Hartree-Fock-Slater options of the CATS code and within the parametric potential FAC code. Calculations of the ground state shift for the AlXII–AlVIII ions have been performed with both codes and fairly agree. Within the Uniform Electron Gas Model, the results from CATS in HF and HFS forms and FAC codes fairly agree together and also agree with the MCDF values from Saha *et al* [18]. Finally a comparison with experimental data on titanium at the ASTRA terawatt laser facility [25] leads to predictions of electron density and temperature in agreement with another interpretation using the MARIA code [38]. In the near future, we intend to apply the present ion-sphere formalism to collisional-radiative modeling.

ACKNOWLEDGMENTS

[1] J. C. Stewart and K. D. Pyatt, Jr., Astrophys. J. **144**, 1203 (1966).

[2] M. Belkhiri and M. Poirier, High Energy Density Phys. **9**, 609 (2013).

[3] M. Belkhiri and M. Poirier, Phys. Rev. A **90**, 062712 (2014).

[4] M. Belkhiri, *Plasma out of thermodynamical equilibrium: influence of the plasma environment on the atomic structure and collisional cross sections*, PhD thesis, Université de Paris XI (2014).

[5] M. F. Gu, Can. J. Phys. **86**, 675 (2008).

[6] J. Abdallah Jr, R. E. H. Clark, J. M. Peek, and C. J. Fontes, J. Quant. Spectrosc. Radiat. Transfer **51**, 1 (1994).

[7] C. J. Fontes, H. L. Zhang, J. Abdallah Jr, R. E. H. Clark, D. P. Kilcrease, J. Colgan, R. T. Cunningham, P. Hakel, N. H. Magee, and M. E. Sherrill, Journal of Physics B: Atomic, Molecular and Optical Physics **48**, 144014 (2015).

[8] R. D. Cowan, *The Theory of Atomic Structure and Spectra* (University of California Press, Berkeley, 1981).

[9] P. Debye and E. Hückel, Phys. Z. **24**, 185 (1923).

[10] D. Salzmann, *Atomic Physics in Hot Plasmas*, The International Series of Monographs on Physics (Oxford University Press, Oxford, 1998).

[11] H. Nguyen, M. Koenig, D. Benredjem, M. Caby, and G. Coulaud, Phys. Rev. A **33**, 1279 (1986).

[12] C. A. Iglesias and R. W. Lee, Journal of Quantitative Spectroscopy and Radiative Transfer **58**, 637 (1997).

[13] R. P. Feynman, N. Metropolis, and E. Teller, Phys. Rev. **75**, 1561 (1949).

[14] B. F. Rozsnyai, Phys. Rev. A **5**, 1137 (1972).

[15] D. A. Liberman, Phys. Rev. B **20**, 4981 (1979).

[16] B. L. Whitten, N. F. Lane, and J. C. Weisheit, Phys. Rev. A **29**, 945 (1984).

[17] D. Salzmann and H. Szichman, Phys. Rev. A **35**, 807 (1987).

[18] B. Saha and S. Fritzsche, J. Phys. B: At., Mol. Opt. Phys. **40**, 259 (2007).

[19] S. Bhattacharyya, A. N. Sil, S. Fritzsche, and P. K. Mukherjee, Eur. Phys. J. D **46**, 1 (2008).

[20] A. N. Sil, J. Anton, S. Fritzsche, P. K. Mukherjee, and B. Fricke, Eur. Phys. J. D **55**, 645 (2009).

[21] D. Mihalas, *Stellar Atmospheres*, 2nd ed., Series of Books in Astronomy and Astrophysics (W. H. Freeman, San Francisco, 1978).

[22] P. Quarati and A. M. Scarfone, Astrophys. J. **666**, 1303 (2007).

[23] R. Piron, *Atome moyen variationnel dans les plasmas quantiques (Variational Average-Atome in Quantum Plasmas,VAAQP)*, PhD thesis, Ecole Polytechnique (2009).

[24] T. Blenski and B. Cichocki, Phys. Rev. E **75**, 056402 (2007).

[25] F. Y. Khattak, O. A. M. B. Percie du Sert, F. B. Rosmej, and D. Riley, Journal of Physics: Conference Series **397**, 012020 (2012).

[26] F. Rosmej, K. Bennadji, and V. S. Lisitsa, Phys. Rev. A **84**, 032512 (2011).

[27] B. F. Rozsnyai, Phys. Rev. A **43**, 3035 (1991).

[28] R. Latter, Phys. Rev. **99**, 510 (1955).

[29] M. Goano, Solid-State Electronics **36**, 217 (1993).

[30] S. Ichimaru, Rev. Mod. Phys. **54**, 1017 (1982).

[31] A. Kramida, Yu. Ralchenko, J. Reader, and NIST ASD Team, NIST Atomic Spectra Database (ver. 5.2), [Online]. Available: `http://physics.nist.gov/asd` [2015, April 29]. National Institute of Standards and Technology, Gaithersburg, MD. (2014).

[32] G. Massacrier and J. Dubau, J. Phys. B: At. Mol. Opt. Phys. **23**, 2459S (1990).

[33] Y.-K. Kim, F. Parente, J. P. Marques, P. Indelicato, and J. P. Desclaux, Phys. Rev. A **58**, 1885 (1998).

[34] P. Beiersdorfer, M. Bitter, S. von Goeler, and K. W. Hill, Phys. Rev. A **40**, 150 (1989).

[35] C. T. Chantler, M. N. Kinnane, J. D. Gillaspy, L. T. Hudson, A. T. Payne, L. F. Smale, A. Henins, J. M. Pomeroy, J. N. Tan, J. A. Kimpton, E. Takacs, and K. Makonyi, Phys. Rev. Lett. **109**, 153001 (2012).

[36] J. T. Larsen and S. M. Lane, J. Quant. Spectrosc. Radiat. Transfer **51**, 179 (1994).

[37] D. Riley, J. Quant. Spectrosc. Radiat. Transfer **60**, 221 (1998).

[38] F. B. Rosmej, J. Phys. B: At., Mol. Opt. Phys. **30**, L819 (1997).

Appendix A: sensitivity of the numerical grid

We have implemented a method to modify the radial grid of CATS so that a point in the grid will correspond to R_0. By default, the grid spacing of CATS is

$$\Delta_r = \alpha * c_Z. \tag{A1}$$

where α is a fixed numerical with a default value of 0.0025. The parameter c_Z is given by

$$c_Z = \frac{1}{4}\left(\frac{2Z}{9\pi^2}\right)^{-1/3}, \tag{A2}$$

where Z is the nuclear charge. When the ion-sphere potential is taken into account, the variable α is adapted so that the grid contains a point that corresponds to R_0. If the grid does not contain R_0, the missing contribution associated with the integrand between the grid point that immediately precedes R_0 and R_0 itself is obtained by linearly interpolating the integrand between the two grid points that straddle R_0. In most cases, the interpolation method that uses the default grid is sufficiently accurate. In Figure 3 we plot the difference between the plasma potential obtained with the linear interpolation method and the case with R_0 on the grid. In that figure we have selected the worst scenario, where the ion-sphere radius is in the middle of two points of the default grid. As can be seen the difference between the two cases is fairly small.

This small change in the plasma potential has a very small impact on the level energy. For instance, in the case of the $1s^2$ ground state of He-like Al, the relative error in the
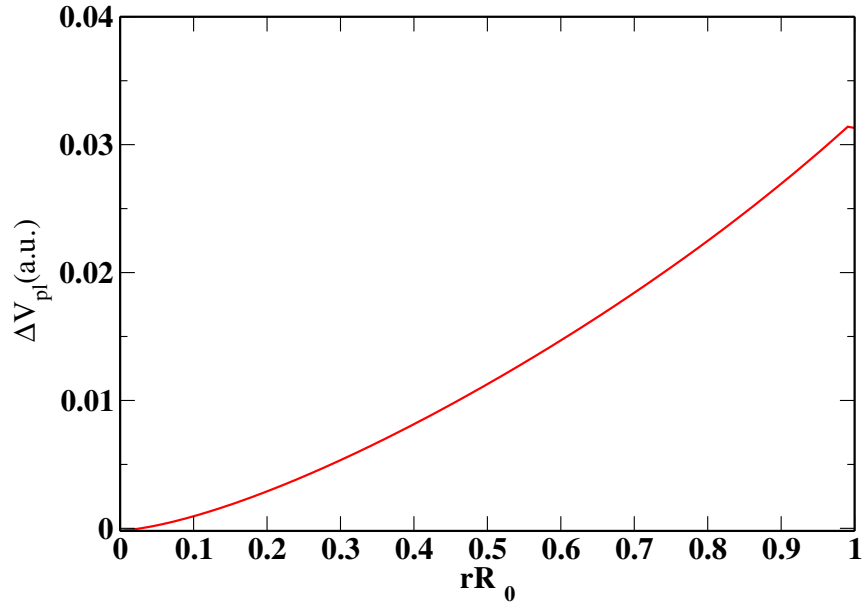
23

FIG. 3. Difference between the plasma potential obtained with the linear interpolation method and the case with R_0 on the grid. The density used is $N_e = 5.1829 \times 10^{23}$ cm^{-3} and the temperature $kT_e = 100$ eV. The electron distance to the nucleus, r, is expressed in units of the ion-sphere radius $R_0 = 3.2457\ a_0$.

energy is 1.344×10^{-6}.